american physiological society

JNP JOURNAL OF NEUROPHYSIOLOGY

J Neurophysiol 132: 277–289, 2024.
First published June 12, 2024; doi:10.1152/jn.00049.2024

RESEARCH ARTICLE

Neuroscience of Disease

Prefrontal cortical network dysfunction from acute neurotoxicant exposure

Michael P. Sceniak and Shasta L. Sabo

Department of Biology, Central Michigan University, Mount Pleasant, Michigan, United States

Abstract

Prefrontal cortical (PFC) dysfunction has been linked to disorders exhibiting deficits in cognitive performance, attention, motivation, and impulse control. Neurons of the PFC are susceptible to glutamatergic excitotoxicity, an effect associated with cortical degeneration in frontotemporal disorders (FTDs). PFC susceptibility to environmental toxicant exposure, one possible contributor to sporadic FTD, has not been systematically studied. Here, we tested the ability of a well-known environmental neurotoxicant, methylmercury (MeHg), to induce hyperexcitability in medial prefrontal cortex (mPFC) excitatory pyramidal neurons, using whole cell patch-clamp recording. Acute MeHg exposure (20 μM) produced significant mPFC dysfunction, with a shift in the excitatory to inhibitory (E-I) balance toward increased excitability. Both excitatory postsynaptic current (EPSC) and inhibitory postsynaptic current (IPSC) charges were significantly increased after MeHg exposure. MeHg increased EPSC frequency, but there was no observable effect on IPSC frequency, EPSC amplitude or IPSC amplitude. Neither evoked AMPA receptor- nor NMDA receptor-mediated EPSC amplitudes were affected by MeHg. However, excitatory synapses experienced a significant reduction in paired-pulse depression and probability of release. In addition, MeHg induced temporal synchrony in spontaneous IPSCs, reflecting mPFC inhibitory network dysfunction. MeHg exposure also produced increased intrinsic excitability in mPFC neurons, with an increase in action potential firing rate. The observed effects of MeHg on mPFC reflect key potential mechanisms for neuropsychological symptoms from MeHg poisoning. Therefore, MeHg has a significant effect on mPFC circuits known to contribute to cognitive and emotional function and might contribute to etiology of neurodegenerative diseases, such as FTD.

NEW & NOTEWORTHY Prefrontal cortical neurons are highly susceptible to glutamatergic excitotoxicity associated with neuronal degeneration in frontal dementia and to environmental toxicant exposure, one potential contributor to FTD. However, this has not been systematically studied. Our results demonstrate that methylmercury exposure leads to hyperexcitability of prefrontal cortical neurons by shifting excitatory to inhibitory (E-I) balance and raising sensitivity for spiking. Our results provide a mechanism by which environmental neurotoxicants may contribute to pathogenesis of diseases such as FTD.

EPSC; glutamate; methylmercury; prefrontal cortex; synapse

INTRODUCTION

Mercury is an environmental toxicant derived from both natural and anthropogenic sources, including the burning of coal, waste incineration and small-scale gold mining (1). Mercury is a heavy metal element and therefore does not degrade. Ongoing industrial environmental release of Hg produces an ever increasing level of potential human exposure (1–4). Exposure to mercury also occurs through hazardous waste. As of 2022, mercury ranked third on the US Agency for Toxic Substances and Disease Hazardous Substance Priority List, based on a combination of the frequency, toxicity, and potential for human exposure at Superfund sites on the National Priorities List (www.atsdr.cdc.gov). Historic examples of large-scale acute mercury poisoning occurred in Minamata, Japan (1953–1956) and Iraq (1970s) (3, 5, 6).

The organic form of Hg, methylmercury (MeHg), is particularly toxic because it is readily absorbed by the skin and gastrointestinal tract (7–10). Methylation by sulfate-reducing bacteria in bodies of water converts elemental Hg to MeHg (1, 2, 11). MeHg binds to free cysteine and proteins containing cysteine and is recognized by the body as methionine (12–14). MeHg is especially insidious, because it is transported across

Correspondence: M. P. Sceniak (michael.sceniak@gmail.com).
Submitted 31 January 2024 / Revised 20 May 2024 / Accepted 5 June 2024

the blood-brain barrier and is not readily eliminated by the body (9). As a result, MeHg bioaccumulates in humans and animals exposed to it over time, producing an additive effect from even low-concentration exposure (15–17). Humans are exposed to MeHg primarily through the consumption of contaminated fish (1, 2, 11, 18–22).

Both organic MeHg and inorganic elemental Hg are associated with cognitive impairment (15, 23–25). Inorganic Hg is known to produce erethism, or "Mad Hatter's disease," a neuropsychological condition associated with significant neurological deficits, including irritability, depression, apathy, and timidity. In extreme cases, affected individuals also experience delirium, personality changes, memory loss, and impaired social interactions. Organic MeHg poisoning is associated with chronic central nervous system impairment, including motor, sensory, and cognitive dysfunction (1, 15, 23, 24). Neuropsychiatric symptoms of MeHg exposure overlap those of elemental mercury, including memory impairment, mood changes, and confusion (15, 23–25). In addition, MeHg exposure has been linked with cognitive impairment and dementia (15, 26). Although it is known that MeHg targets the brain (27–29) more effectively than inorganic mercury (15, 30), little is known about the neural mechanisms that give rise to these complex neuropsychological symptoms in MeHg exposure.

MeHg exposure may also contribute to diseases such as frontotemporal dementia or frontotemporal disorders (FTD), which exhibit cognitive dysfunction with substantial overlap with MeHg exposure. Fifty to 70% of FTD cases are sporadic, with no identified genetic cause (31–35). Risk genes associated with FTD, such as TDP-43, are not sufficient to account for all PFC disorders (31). This has led to the hypothesis that gene-environment interactions (gXe) combine to attack a common target, such as prefrontal cortical circuits, leading to their dysfunction (36–38). MeHg is a strong candidate for the environmental factor that could lead to these diseases. Bioaccumulation would result in conditions that effectively increase mercury exposure over time. This time course is consistent with cognitive diseases affecting the adult or aging prefrontal cortex, leading to dementia and cognitive impairment, with symptoms increasing with age (36–38).

Despite the strong association of MeHg exposure with cognitive dysfunction (15, 17, 25), little is known about the neural mechanisms associated with neocortical dysfunction. MeHg exposure leads to bioaccumulation specifically in the neocortex, including cingulate and frontal cortex (15–17). Neocortical bioaccumulation of MeHg results in altered cognitive and emotional function prior to neurodegeneration or gross morphological brain changes (25, 39, 40). Outside the prefrontal cortical (PFC), MeHg exposure is known to produce synaptic disruption not observable with gross morphological methods (41, 42). Therefore, we have used electrophysiological methods to show that MeHg differentially affects excitatory and inhibitory synaptic pathways of prefrontal circuits to promote hyperexcitability dysfunction by shifting the excitatory to inhibitory (E-I) balance toward excitation.

MeHg exposure is unavoidable in the modern world and is likely to increase in the future. Bioaccumulation from MeHg exposure means that even low levels could sum over one's lifetime. In addition, low levels that do not promote neuronal cell death could disrupt cognitive function or interact with genetic risks to trigger cognitive dysfunction. Understanding MeHg effects on circuits involved with cognitive function will not only help explain dysfunction related to MeHg exposure but also shed light on possible contributions to sporadic cases of dementia and cognitive impairment, such as FTD.

METHODS

All procedures and protocols used in this study adhere to published guidelines of the National Institutes of Health and were approved by the Institutional Animal Care and Use Committee at Central Michigan University or Michigan State University.

Preparation of Acute Prefrontal Cortical Brain Slices

Mouse cortical slices were cut from young adult (25–28 days postnatal) mice (C57BL/6J). All mice used in the study were young males to provide a consistent population of healthy neurons and to avoid effects of estrus. Initially, mice were deeply anesthetized with isoflurane (>5%) and received a transcardioperfusion with artificial cerebral spinal fluid (ACSF) containing NMDG (*N*-methyl-D-glucamine) and HEPES (4-(2-hydroxyethyl)-1-piperazineethanesulfonic acid) buffer, before dissection of the whole brain. The brain was temporarily (<30 s) placed in ice-cold (1–4°C) oxygenated (95% O2, 5% CO_2) NMDG-HEPES ACSF (43), composed of the following (in mM): 92 NMDG, 2.5 KCl, 1.25 NaH_2PO_4, 30 $NaHCO_3$, 20 HEPES, 25 D-glucose, 2 thiourea, 5 Na-ascorbate, 3 Na-pyruvate, 0.5 $CaCl_2$, and 10 $MgSO_4$. Next, the brain was cut into a block containing the mPFC and glued to platform supported by solid agar gel (4%). Neocortical brain slices were then cut in oxygenated ice-cold NMDG-HEPES ASCF into 300-μm thick slices and placed in a holding chamber with 30–35°C HEPES ACSF that gradually (<30 min) equilibrated to room temperature (25°C). HEPES ACSF contained the following (in mM): 92 NaCl, 2.5 KCl, 1.25 NaH_2PO_4, 30 $NaHCO_3$, 20 HEPES, 25 glucose, 2 thiourea, 5 Na-ascorbate, 3 Na-pyruvate, 2 $CaCl_2$, and 2 $MgSO_4$. Brain slices were transferred from the holding chamber after 1–2 h and placed in a submersion-recording chamber. Slices were perfused with oxygenated 30–35°C gravity-fed normal ACSF (2–4 mL/min) composed of the following (in mM): 126 NaCl, 1 NaH_2PO_4, 25 $NaHCO_3$, 25 D-glucose, 3 KCl, 2 $MgSO_4$ and 2 $CaCl_2$. Neurons were visualized using a Nikon Eclipse E600FN microscope (Nikon Instruments Inc., Melville, NY) equipped with a water immersion objective (×40) with infrared wavelength illumination, differential interference contrast optics (DIC) and a Sony IR-1000 CCD camera (DAGE MTI, Michigan City, IN) with contrast enhancement.

Whole Cell Recording in Prefrontal Cortical Slices

Membrane potentials and currents were collected using either a Multi-clamp 700A or 700B patch clamp amplifier (Axon Instruments, Foster City, CA) and digitized using a Digidata 1440A analog-to-digital converter which was controlled by the pClamp 10.2 software package (Axon Instruments). In order to measure intrinsic membrane properties and spiking activity, recording electrodes were filled with a K-gluconate-based internal solution (41, 44, 45) composed of the following (in mM):

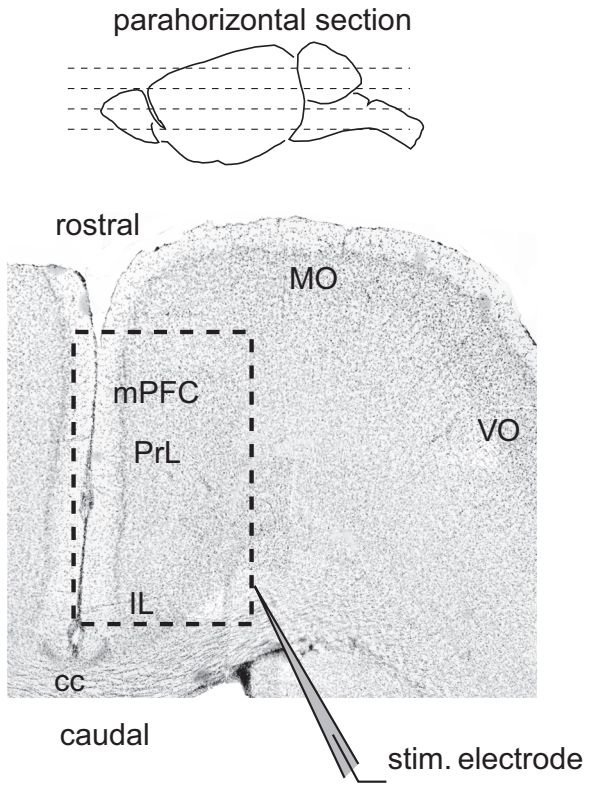

Figure 1. Illustration of parahorizontal brain slice. Representative low-magnification (×4) image of medial prefrontal cortex (mPFC) brain slice used to record neurons in the study. The parahorizontal section contains a large region of mPFC prelimbic (PrL) neurons and preserves the laminar structure of the cortical region. The corpus callosum (cc), infralimbic (IL), medial orbital (MO), and ventral orbital (VO) brain regions are labeled for reference. Electrical stimulation via current pulses was achieved with a bipolar stimulating electrode positioned in the white matter projecting to the mPFC.

100 K-gluconate, 20 KCl, 10 phosphocreatine, 5 $MgCl_2$, 10 HEPES, 4 Na-ATP, 0.3 Na-GTP (pH 7.3 and 290–300 mosmol/L). Membrane potential recordings of action potentials were recorded in current-clamp mode, corrected for the liquid junction potential, while synaptic currents were recorded in voltage-clamp mode. Spontaneous excitatory synaptic currents (EPSCs) were recorded (46), using the following Cs-methylsulfonate internal electrode solution (in mM): 120 Cs-methylsulfonate, 12 CsCl, 0.1 EGTA, 2 $MgCl_2$, 10 HEPES, 2 Na-ATP, 0.25 Na-GTP, 10 phosphocreatine and 5 QX314 (pH 7.3 and 290–300 mosmol/L). Spontaneous inhibitory synaptic currents (IPSCs) were recorded, using the following CsCl internal electrode solution (in mM): 130 CsCl, 5 $MgCl_2$, 0.2 EGTA, 10 HEPES, 4 Na-ATP, 0.3 Na-GTP, 10 phosphocreatine and 5 QX314 (pH 7.3 and 290–300 mosmol/L). Electrode resistance ranged from 4–8 MΩ when filled with internal pipette solution. Recordings were considered successful if the resting membrane potential was −57 mV or more negative at initial recording. Recordings with seals <1 GΩ or resting potentials more positive than −57 mV or series resistance higher than 30 MΩ were not included in the analysis.

Only one cell was recorded per slice. All recordings were continuous before and during MeHg application. All cells were recorded for at least 45 min total, allowing us to make within-cell comparisons for before and after MeHg exposure. MeHg was added to normal ACSF to achieve a final concentration of 20 μM. After collecting the baseline recordings, the perfusion was switched to MeHg-containing ACSF. After 15 min of MeHg exposure, recordings were made for comparison to control (pre-MeHg exposure). The MeHg concentration (20 μM) was chosen because it is consistent with concentrations known to produce toxicity in humans and provides a useful time frame for in vitro effects to be observed (1, 41, 42, 47). In addition, this concentration is consistent with previous studies of other types of neurons in the brain and spinal cord, providing the opportunity for direct comparison of the effect of MeHg exposure across neuron types (41, 48–51).

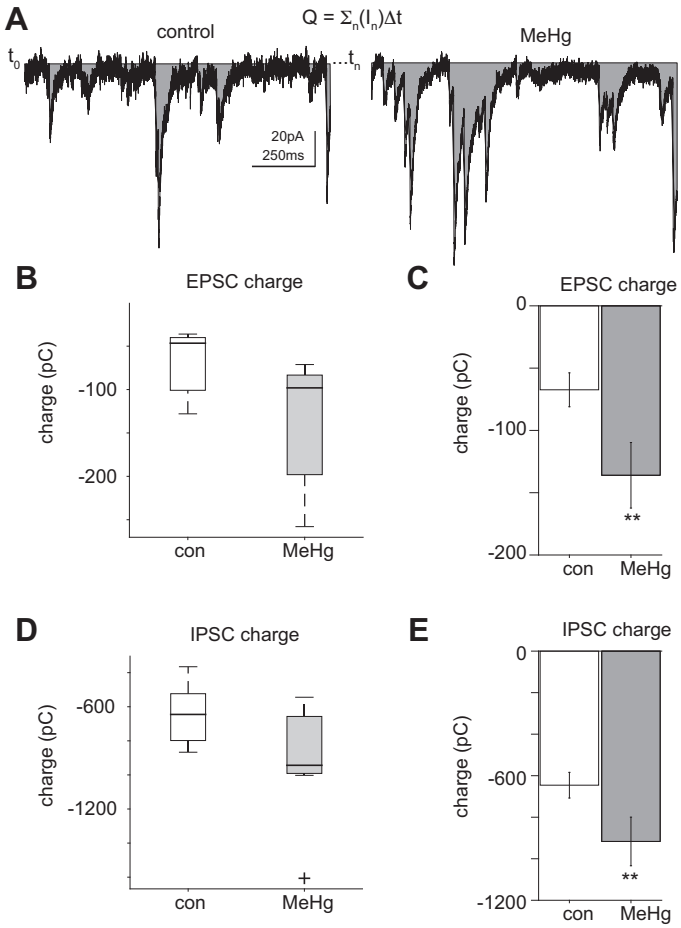

Figure 2. Excitatory and inhibitory synaptic charge were estimated before and after MeHg exposure in mPFC excitatory pyramidal neurons. *A*: illustration of charge measurements for a representative postsynaptic current recording before and after MeHg treatment. Charge is shown as the summed gray region under the curve. Postsynaptic current charge was calculated as the sum of the current response over time to produce the net area under the curve in units of pico coulombs (pC). *B–E*: boxplots are shown to provide illustration of statistical spread of quartiles and outliers. Barplots are also shown for mean estimates. *B* and *C*: across the population of sampled neurons ($n = 10$), the excitatory glutamatergic charge was significantly (indicated by **) increased after MeHg exposure (control = −46 ± 13 pC, MeHg = −98 ± 26 pC; $P = 0.0132$, Wilcoxon ranksum test). *D* and *E*: the inhibitory charge was also significantly increased (indicated by **) after MeHg treatment (control = −645 ± 61pC, MeHg = −943 ± 117 pC; $P = 0.0133$, Wilcoxon ranksum test) across the population of sampled neurons ($n = 11$). EPSC, excitatory postsynaptic current; IPSC, inhibitory postsynaptic current; MeHg, methylmercury; mPFC, medial prefrontal cortex.

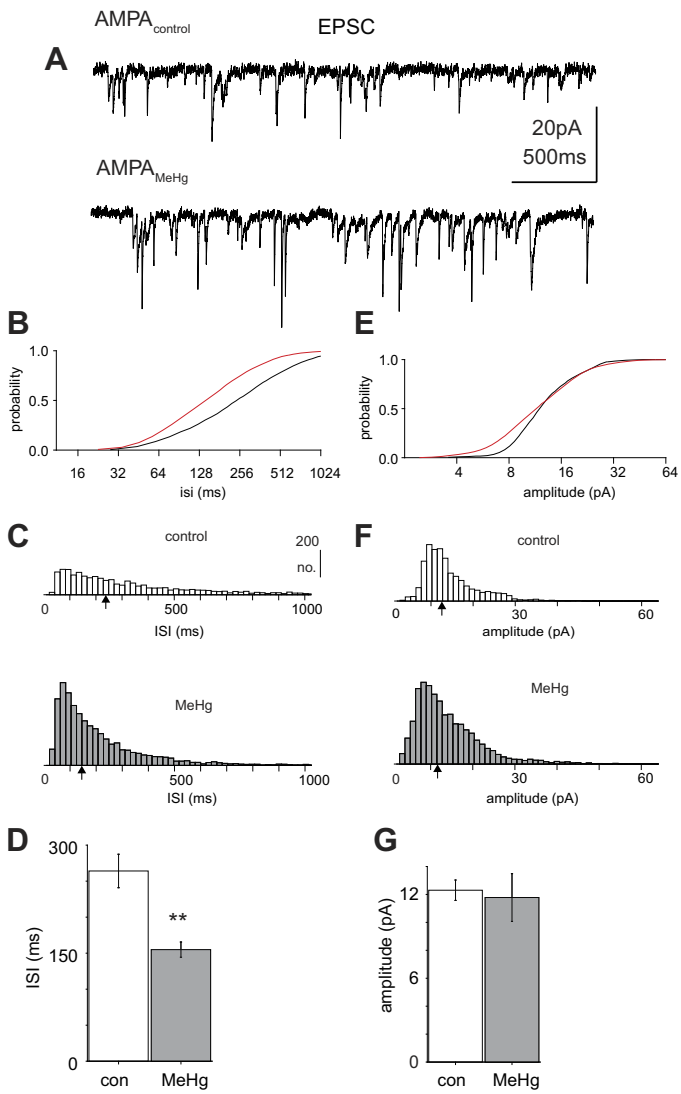

Figure 3. In mPFC excitatory pyramidal neurons, acute MeHg exposure produced increased frequency, but not amplitude, of pharmacologically isolated AMPA EPSCs. *A*: representative current traces of EPSCs recorded in an mPFC neuron before and after MeHg exposure (15 min). *B* and *E*: cumulative distributions for both event ISI and EPSC amplitude were significantly different between control and MeHg conditions (P = 8.6e-42; P = 7e-98 for amplitude and ISI respectively; Kolmogorov–Smirnov test, n = 11 neurons). *C* and *D*: EPSC event ISI (inverse of frequency) displayed a consistent significant (indicated by **) reduction across the population of sampled neurons (n = 11). EPSC mean ISI (control = 264 ± 23 ms, MeHg = 154 ± 11) was highly significantly different (P = 0.001004, Wilcoxon rank-sum test), with a consistent increase in EPSC frequency after MeHg exposure. Arrows indicate distribution median. *F* and *G*: across the population (n = 11 neurons), the mean amplitude of EPSCs was not significantly affected by MeHg (control = 12.3 ± 0.7 pA, MeHg = 11.8 ± 1.7 pA). The significant difference in the cumulative distribution reflects an increase in smaller EPSC events as frequency increases, without a shift in the mean amplitude. EPSC, excitatory postsynaptic current; ISI, intersynaptic interval; MeHg, methylmercury; mPFC, medial prefrontal cortex.

EPSCs and IPSCs

Recordings of AMPA receptor-mediated currents were made using whole cell voltage-clamp techniques (V_{hold} = −60 mV) in normal ACSF in the presence of the GABAergic blocker picrotoxin (100 μM). GABAergic IPSCs were collected (V_{hold} = −70 mV) in the presence of glutamate receptor antagonists, CNQX (10 μM; 6-cyano-7-nitroquinoxaline-2,3-dione) and APV (50 μM; (2 R)-amino-5-phosphonovaleric acid).

Electrical Stimulation

Electrical evoked responses were achieved, using bipolar electrodes placed in the white matter projecting to the adjacent neurons of the medial prefrontal cortex (mPFC). Temporal synchronized current pulses were delivered through the bipolar electrodes to evoke synaptic responses. Seven to ten repeats

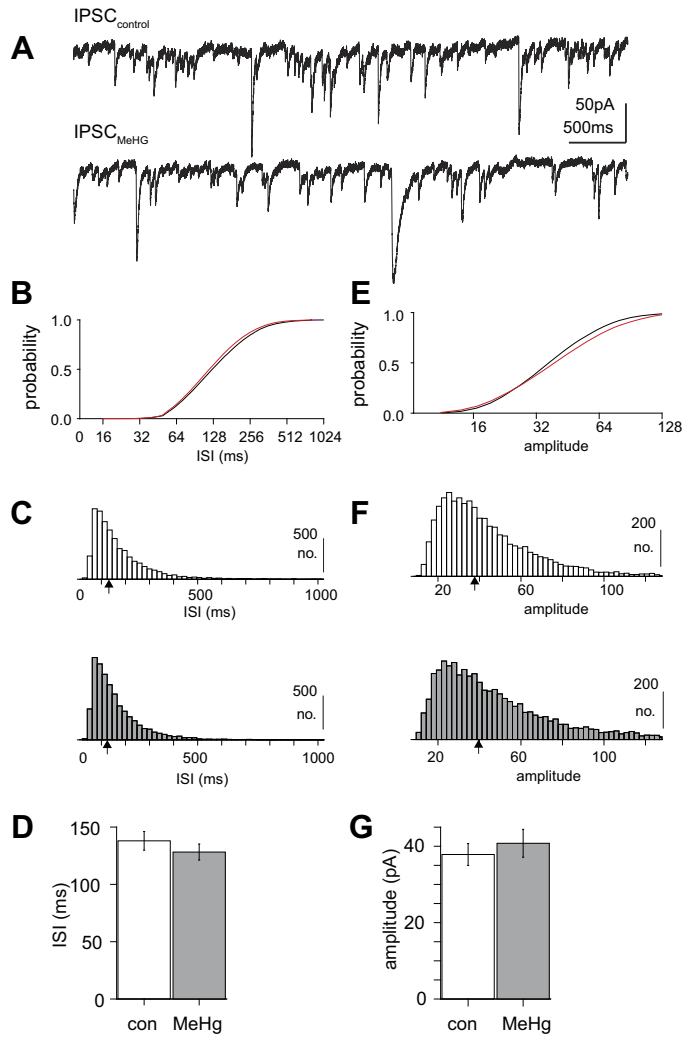

Figure 4. Acute MeHg does not alter spontaneous inhibitory synaptic event frequency or amplitudes in mPFC excitatory pyramidal neurons. *A*: representative IPSC recording traces both before and after (15 min) MeHg exposure. *B* and *E*: both IPSC event ISI and amplitude show significant differences (P = 2.6e-6, P = 5e-14 for ISI and amplitude, respectively; Kolmogorov–Smirnov test) in their cumulative distributions across the population of sampled mPFC pyramidal neurons (n = 10), reflecting small differences in the inhibitory synaptic event composition. However, the mean population statistics show no significant difference. *C* and *D*: across the population (n = 10) IPSC event ISI (control = 37.8 ± 3 ms, MeHg = 40.8 ± 3.6 ms) were statistically identical, indicating that frequency was not significantly increased by MeHg exposure (control = 7.2 ± 0.4 Hz, MeHg = 7.8 ± 0.4 Hz). Arrows indicate distribution median. *F* and *G*: IPSC event amplitude was also not significantly altered by MeHg treatment (control = 37.8 ± 3 pA, MeHg = 40.8 ± 3.6 pA). IPSC, inhibitory postsynaptic current; ISI, intersynaptic interval; MeHg, methylmercury; mPFC, medial prefrontal cortex.

of currents were delivered with sufficient temporal delay (15 s) to avoid adaptation. Mean synaptic responses were estimated across repeats.

Analysis of Action Potential Dynamics and Input-Output Curves

Voltage measurements were collected using current-clamp of layer 5 excitatory pyramidal neurons. Action potentials were identified based on voltage deviation above the threshold (>10 mV). The time of occurrence of action potentials was determined as peak voltage. Firing rates were estimated over 3 s. Quantification of f-I curves was estimated based on action potential firing rate versus injected current pulse amplitude (pA). Each current step was presented once, with a 15 s blank between steps. Spontaneous background firing rates were determined during periods of no current injection over a defined temporal period.

Data Analysis

Offline data analysis was performed on time-locked current or voltage responses. Intrinsic membrane properties were estimated through pClamp and postprocessing using custom-written analysis routines in Matlab. All data are expressed as the means ± SE unless otherwise stated. All within-subject analyses used paired comparisons. Statistical significance was determined using either the Wilcoxon rank-sum test with P value given by the Mann–Whitney U test for nonparametric data or the Kolmogorov–Smirnov test for cumulative distributions. Estimates were considered significant at $P \leq 0.05$.

RESULTS

Methylmercury Exposure Differentially Affects mPFC Excitatory and Inhibitory Synaptic Activity

To understand how mercury exposure affects prefrontal cortical circuit function, we first asked whether mercury exposure alters synaptic properties of excitatory pyramidal neurons in prelimbic mPFC. To record excitatory and inhibitory synaptic responses, whole cell patch-clamp recordings were performed in acute parahorizontal mouse brain slices (Fig. 1). Since they are made normal to the mPFC surface, parahorizontal slices provide optimal preservation of pyramidal neuron dendrites and afferent inputs and produce active mPFC networks (46). Pyramidal neurons within layer 5 were targeted for recording. In all cases, responses were compared in the same neuron before and after 15 min exposure to MeHg (20 μM bath application). Based on previous studies, 20 μM MeHg shows significant effects within 15 min of bath application, which allows for before and after recording of neurons within the time span allowed by the brain slice preparation. This concentration is also consistent with acute toxicity known to produce symptoms observed in humans (1, 15, 23).

To estimate overall levels of spontaneous excitatory and inhibitory synaptic activity, synaptic charge was estimated for pharmacologically isolated excitatory and inhibitory currents (Fig. 2). Synaptic current charge is estimated as the integrated area under the curve, for either excitation or inhibition, over a given time sample. An example of synaptic

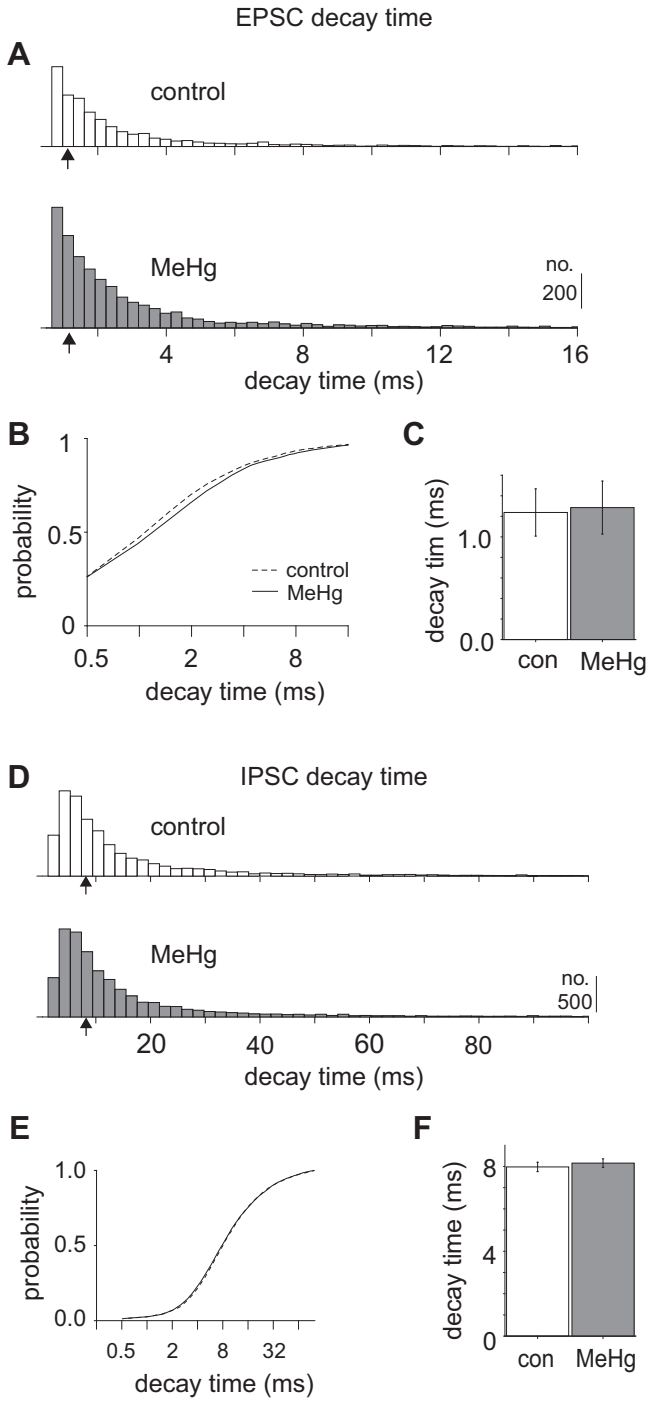

Figure 5. Neither EPSC nor IPSC event decay times were significantly affected by MeHg treatment. *A–C*: EPSC event decay times for control (1.24 ± 0.23 ms) were statistically identical to MeHg treated estimates (1.28 ± 0.26 ms). However, the cumulative distributions were significantly different (P = 4.5e-4, Kolmogorov–Smirnov test), indicating a shift in the shapes of the decay distributions. *D–F*: similarly, IPSC event decay times were not significantly different for control (7.9 ± 0.22 ms) vs. MeHg treated conditions (8.2 ± 0.2 ms). The cumulative distributions for IPSCs were also not significantly different. EPSC, excitatory postsynaptic current; IPSC, inhibitory postsynaptic current; MeHg, methylmercury.

charge estimation is shown in Fig. 2*A*. Synaptic current charge allows estimation of glutamatergic and GABAergic synaptic activity, regardless of the source of potential activity changes (e.g., changes in synaptic response amplitude, frequency, kinetics, or temporal organization).

For both excitation and inhibition, synaptic charge was markedly increased in the presence of MeHg compared with control (Fig. 2). Across the population of sampled neurons, mean excitatory synaptic charge (Fig. 2, *B* and *C*) was significantly increased after MeHg exposure (−67 ± 13 pA and −136 ± 26 pA, control and MeHg exposure, respectively; n = 10 neurons; $P = 0.0013$, Wilcoxon ranksum). Mean inhibitory charge (Fig. 2, *D* and *E*) was also significantly increased after MeHg exposure (−646 ± 61 pA and −917 ± 116 pA, control vs. MeHg; $n = 11$ neurons; $P = 0.013$, Wilcoxon ranksum).

Since excitatory synaptic activity was increased, individual synaptic responses were analyzed to determine whether increased excitatory charge results from changes in the frequency and/or amplitudes of spontaneous EPSCs (Fig. 3). To do so, fast excitatory glutamatergic AMPA currents were recorded using a Cs-methylsulfonate internal electrode solution and normal ACSF (see METHODS) containing picrotoxin (100 μM) to suppress GABAergic responses. After MeHg exposure, AMPA currents displayed a significant increase in their rate of occurrence, across the population of sampled neurons (Fig. 3, *B–D*; $n = 11$). The distribution of AMPA EPSC intersynaptic interval (ISI) was significantly shifted (Fig. 3, *B* and *C*; P = 7.0655e-98, Kolmogorov–Smirnov test). Consistent with this left-ward shift in the ISI distribution, the frequency of AMPA EPSC events was significantly increased (P = 0.001004, Wilcoxon ranksum test) after MeHg exposure (6.5 ± 0.5 Hz) compared with control (3.7 ± 0.3 Hz). Although the cumulative distributions were significantly different for amplitude (P = 8.67e-42, Kolmogorov–Smirnov test; Fig. 3*E*), the mean EPSC amplitudes were not significantly different before (12 ± 0.7 pA) and after (11.78 ± 1.7 pA) MeHg exposure (Fig. 3, *F* and *G*). MeHg appears to bias the EPSC amplitude distribution toward an increase in smaller amplitude events. This explains the change in the shape in the cumulative distribution; however, the increased variability in amplitude appears to make the overall mean non-significant between control and MeHg-treated AMPA-based EPSCs (Fig. 3, *F* and *G*).

To understand whether changes in IPSC frequency and/or amplitude underlie increased inhibitory synaptic charge, inhibitory GABAergic synaptic currents were recorded using pharmacological blockage of EPSCs via CNQX and APV (see METHODS). In addition, IPSCs were amplified by reversing the chloride gradient through use of a CsCl-based internal recording electrode solution. Surprisingly, neither IPSC amplitude (37.8 ± 2.9 pA and 40.7 ± 3.6 pA before and after MeHg, respectively) nor frequency of synaptic events (7.2 ± 0.4 Hz and 7.8 ± 0.4 Hz before and after MeHg) was significantly different across the population (n = 10) of recorded neurons (Fig. 4). Although the ISI distributions appeared similar before and after MeHg treatment, a small leftward shift was statistically significant (P = 2.6504e-06, Kolmogorov–Smirnov test; Fig. 4*B*). Consistent with this limited change in the ISI distribution, the mean synaptic event ISIs were not significantly different after mercury exposure (Fig. 4, *C* and *D*). Similarly, the cumulative distributions of IPSC amplitude were statistically different before and after MeHg exposure

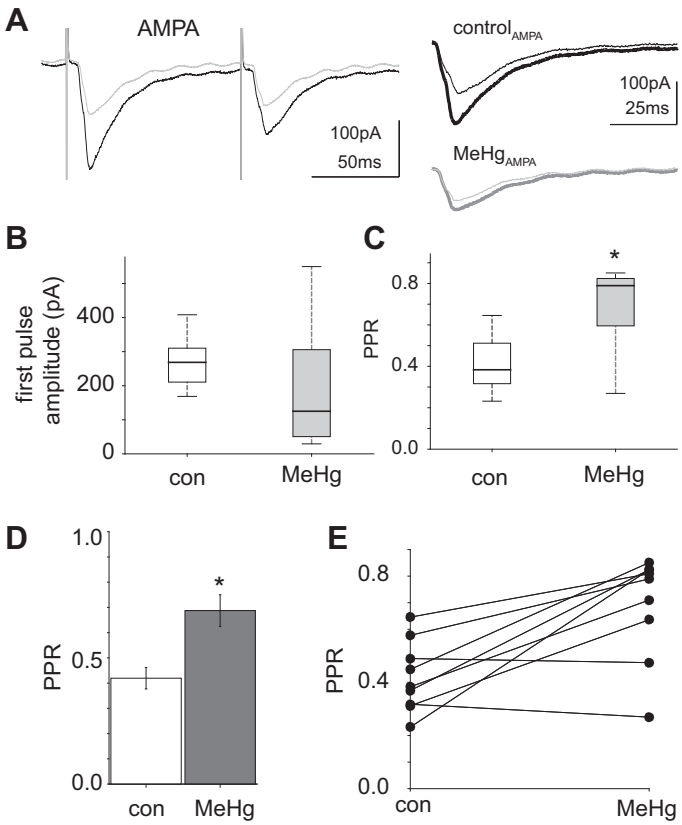

Figure 6. Representative electrically evoked AMPA current response in an mPFC excitatory pyramidal neuron before and after MeHg treatment. *A*: control (black) current trace shown overlapping post-MeHg-exposed (15 min) current trace (gray) for two consecutive white matter evoked responses. *Inset* to the *right* shows illustrations of the first (thick) vs. second (thin) current response for control (black) and MeHg exposed (gray) conditions. *B–E*: evoked AMPA population responses (n = 9) are shown for statistical averages of first EPSC amplitude and EPSC PPR (second/first amplitude ratio) to consecutive electrical stimulus pulses across the sample of neurons recorded in mPFC before (control) and after MeHg treatment. There was no significant difference in median first pulse amplitude (control = 268 ± 24 pA, MeHg = 125 ± 61 pA), but the PPR was significantly (control = 0.38 ± 0.04, MeHg = 0.79 ± 0.07; P = 0.010325, Wilcoxon ranksum test) increased (indicated by *) after MeHg exposure. EPSC, excitatory postsynaptic current; IPSC, inhibitory postsynaptic current; MeHg, methylmercury; mPFC, medial prefrontal cortex; PPR, paired-pulse amplitude ratio.

(P = 4.9777e-14, Kolmogorov–Smirnov test), apparently as a result of fewer high amplitude events after MeHg (Fig. 4*E*). However, the mean amplitudes were not significantly different (Fig. 4, *F* and *G*), consistent with a non-Gaussian distribution of the events, also evident from the histograms of IPSC amplitudes.

Changes in excitatory or inhibitory charge could result from changes in the excitatory or inhibitory synaptic decay time constant, producing either longer or shorter temporal summation. To determine the effects of MeHg on synaptic temporal properties, the decay time constants for excitation and inhibition were also examined (Fig. 5). MeHg show no significant effect on EPSC decay time (1.23 ± 0.23 ms and 1.28 ± 0.26 ms for control and MeHg, respectively), although there was a small, but significant shift in the cumulative distribution (P = 4.5e-4, Kolmogorov–Smirnov test). In addition, there was no significant difference in IPSC decay time constant as a result of MeHg treatment (7.9 ± 0.2 ms and 8.2 ± 0.2

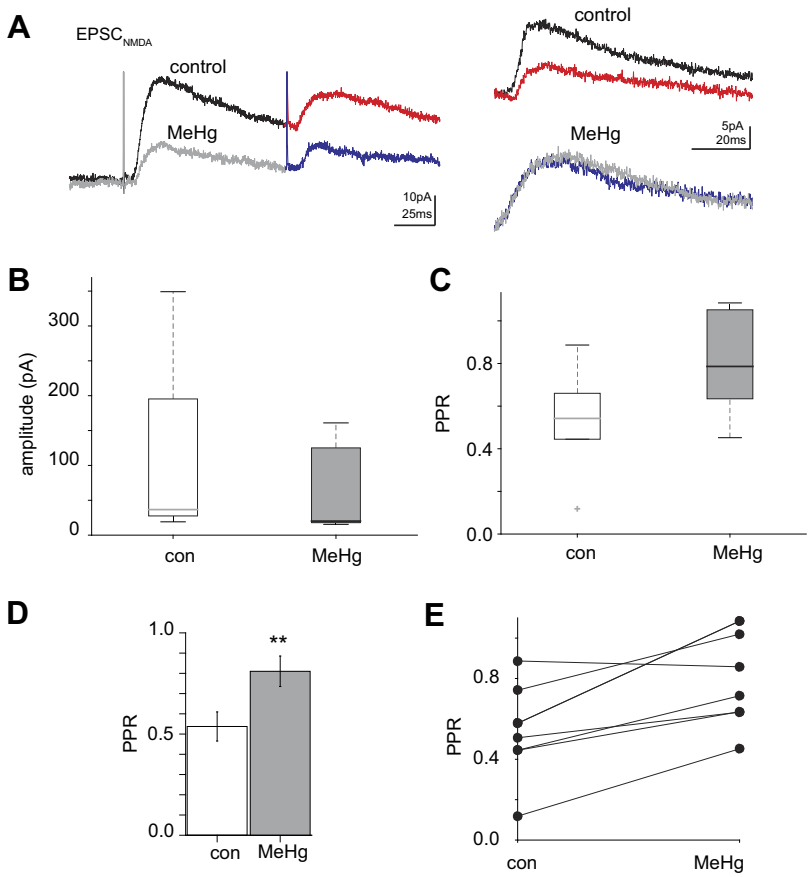

Figure 7. Electrically evoked NMDA responses of excitatory pyramidal mPFC neurons in response to acute MeHg exposure. *A*: representative current trace of a pharmacologically and electrically ($V_{holding}$ = +10 mV) isolated NMDA current both before (black) and after (15 min) MeHg treatment (gray). Paired pulse analysis was achieved through consecutive current pulses stimulating afferent mPFC inputs within the white matter. Paired pulse ratios (second/first pulse) were analyzed for control (red/black) vs. MeHg treated (blue/gray) conditions. *Inset* to the *right* shows first to second overlays for control (first = black, second = red) and MeHg treated (first = gray, second = blue) current recordings. *B*: the first NMDA-evoked current response to the pair of consecutive stimuli was not significantly different (control = 110 ± 42 pA, MeHg = 62 ± 20 pA) across the sampled neurons (n = 7). *C–E*: across the population of sampled neurons (n = 7), the NMDA PPR was significantly (indicated by **) increased (control = 0.53 ± 0.1, MeHg = 0.81 ± 0.1; P = 0.0342, Wilcoxon ranksum test) in excitatory pyramidal mPFC neurons after MeHg exposure. EPSC, excitatory postsynaptic current; IPSC, inhibitory postsynaptic current; MeHg, methylmercury; mPFC, medial prefrontal cortex; NMDA, *N*-methyl-D-aspartate; PPR, paired-pulse amplitude ratio.

ms for control and MeHg, respectively). Therefore, changes in the temporal dynamics of individual synaptic responses cannot account for the increased synaptic charge induced by MeHg exposure.

Methylmercury Exposure Reduces Paired-Pulse Depression and Probability of Release

Since mercury induced an increase in EPSC frequency, we next asked whether this increase in EPSC frequency is a result of increased probability of release. To test this, the effects of MeHg on paired-pulse plasticity were determined (Fig. 6 and Fig. 7) through electrical stimulation of afferent white matter-originating inputs (Fig. 1) and recording of evoked AMPA receptor EPSCs. Consecutive electrical pulses were applied via extracellular bipolar electrode stimulation, to determine paired-pulse amplitude ratios (PPRs). Paired-pulse stimulation was averaged over repeats (n = 7) with sufficiently long delay periods (15 s) to avoid adaptation. Surprisingly, MeHg exposure (Fig. 6*A*, gray) significantly (P = 0.010, Wilcoxon ranksum) altered synaptic plasticity by increasing PPR (0.42 ± 0.04 and 0.69 ± 0.06 control vs. MeHg, Fig. 6, *C–E*). The amplitude of the current response to the first pulse was not significantly different in response to MeHg exposure (270 ± 24 pA vs. 194 ± 61 pA, Fig. 6*B*); however, the variability in the amplitude of the first pulse was increased. The observed increase in PPR suggests that MeHg exposure reduces the probability of release, thereby altering presynaptic plasticity. Given that probability of evoked release decreased, this type of stimulus-evoked synaptic plasticity appears distinct from the increases in spontaneous EPSC frequency induced by MeHg (Fig. 3).

Methylmercury Exposure Does Not Alter NMDA Receptor Responses in mPFC

N-methyl-D-aspartate (NMDA) receptors are abundant at excitatory synapses in mPFC and are thought to play a role in pathogenesis of some forms of cognitive dysfunction and dementia (52–56); therefore, it is important to determine whether NMDA receptor responses are altered by MeHg exposure. To do so, NMDA synaptic currents were recorded in the presence of CNQX, with the cells voltage-clamped at +10 mV holding potential. NMDA synaptic responses were evoked via extracellular bipolar stimulation of afferent inputs originating in the adjacent white matter (Fig. 7, and see Fig. 1). NMDA synaptic currents were then analyzed in response to consecutive pulses, as described above for AMPA receptor responses. The amplitudes of the NMDA synaptic currents (first pulse amplitudes: 110 ± 42 pA vs. 62 ± 20 pA, control vs. MeHg; n = 7 neurons) were not significantly different (Fig. 7, *A* and *B*). Interestingly, the variability of the NMDA synaptic current amplitude to the first pulse was reduced in response to MeHg exposure. There were also no observable changes in the kinetics of the NMDA responses, consistent with no change in NMDA receptor subunit composition. As expected based on what was observed with AMPA synaptic currents, NMDA currents displayed a marked increase in PPR (Fig. 7, *C–E*; P = 0.034, Wilcoxon ranksum; 0.54 ± 0.07 and 0.81 ± 0.08, control vs. MeHg; n = 7).

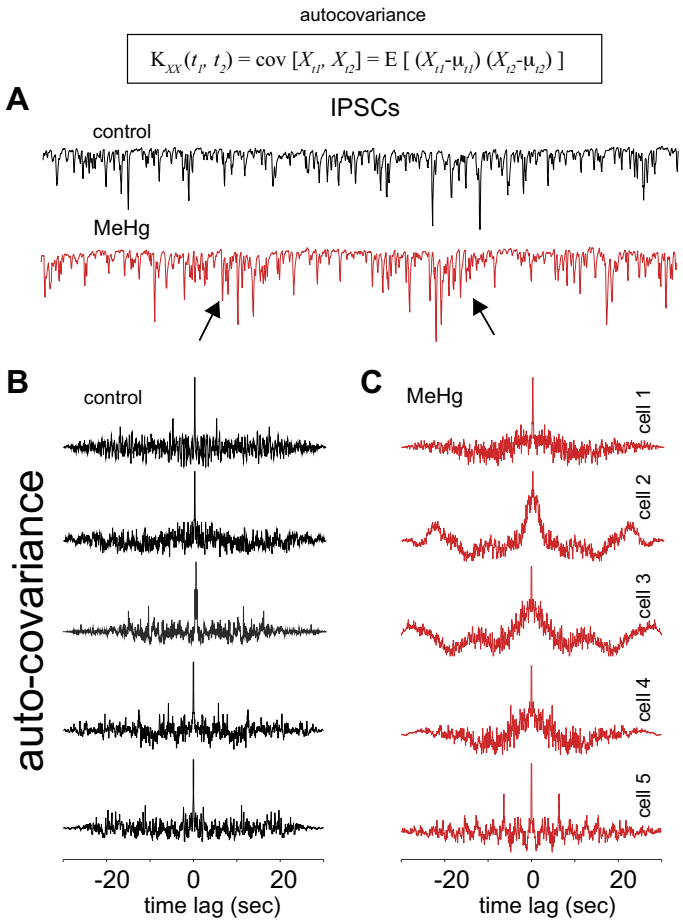

Figure 8. MeHg-induced synchrony is revealed by the autocovariance function of the inhibitory synaptic currents. *A*: representative whole cell voltage-clamp recording of IPSCs in an mPFC pyramidal neuron. The autocovariance function was used to calculate the mean subtracted autocorrelation of the IPSC traces before and after MeHg treatment. Periodic temporal patterns within the IPSC current traces are evident after MeHg treatment through peaks in the autocorrelation at nonzero times. If the IPSC traces were purely random signals, then the autocorrelation would display a peak at time zero and would otherwise be flat. Arrows highlight synchrony within the IPSC traces, resulting in bursting events. *B* and *C*: autocovariance functions are shown for the IPSC current traces of five representative neurons before (black) and after (red) MeHg exposure. IPSC, inhibitory postsynaptic current; MeHg, methylmercury; mPFC, medial prefrontal cortex.

Mercury Exposure Synchronizes mPFC Inhibitory Synaptic Activity

Since the change in inhibitory charge could not be explained by increased IPSC amplitude or frequency, statistical analysis of inhibitory current traces was used to determine whether the temporal structure of GABAergic inhibition is altered by MeHg exposure. This analysis revealed changes in temporal correlation of IPSCs upon mercury exposure (Fig. 8). The mean-subtracted autocorrelation function, also known as the autocovariance, is a useful statistical tool to determine temporal structure within a signal. For a completely random signal, the autocovariance will be simply a peak at zero time delay and otherwise flat at all other time delays (similar to Fig. 8*B*). Figure 8 shows the autocovariance function for the inhibitory current traces of three representative neurons before and after MeHg exposure. In the control condition, the IPSC traces displayed relatively random temporal structure, similar to what has been reported for synaptic events from neocortical ex vivo recordings (Fig. 8*B*). In the presence of MeHg, there was a marked change in the temporal structure of the inhibitory signal (Fig. 8*C*, red curves). The symmetric oscillations observed in the autocovariance functions reveal frequency-specific oscillations in the occurrence of IPSCs after mercury exposure. This reflects a change in the temporal pattern of IPSCs converging onto excitatory pyramidal neurons in mPFC, from random to synchronous, after MeHg exposure. Interestingly, the frequency of the oscillations appears slow for each representative recording (Fig. 8*C*), reflecting slow bursting patterns. This temporal network synchrony represents a unique network perturbation as a result of MeHg exposure that would induce significant changes in neocortical function.

In contrast to IPSCs, EPSCs did not show significant changes in the degree of temporal synchrony, as seen in the autocovariance function (Fig. 9). Although EPSCs showed a significant increase in the frequency of occurrence (Fig. 9*A* and Fig. 3*D*), the autocovariance before and after MeHg exposure is more consistent with a random process (Fig. 9, *B*

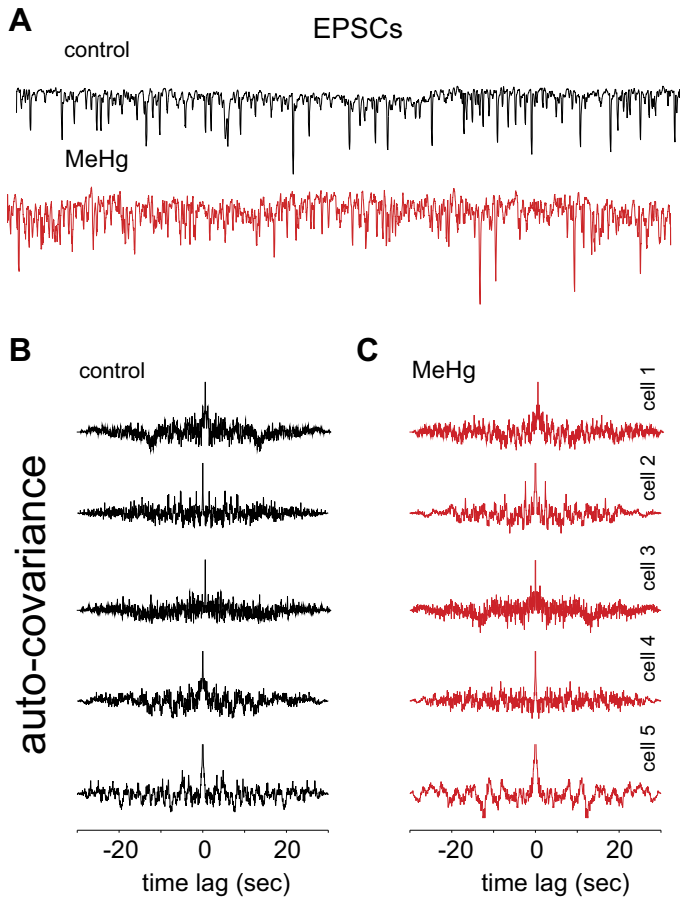

Figure 9. Autocovariance functions for EPSC recordings show no significant changes in temporal synchrony despite increases in mean frequency of events after MeHg treatment. *A*: representative EPSC current recordings for control (black) and MeHg treated (red) conditions in the same mPFC excitatory layer 5 neuron. *B* and *C*: the autocovariance function of EPSC recordings is shown before and after MeHg treatment for five representative neurons. Despite changes in mean frequency, the autocovariance functions are relatively unaffected. EPSC, excitatory postsynaptic current; MeHg, methylmercury; mPFC, medial prefrontal cortex.

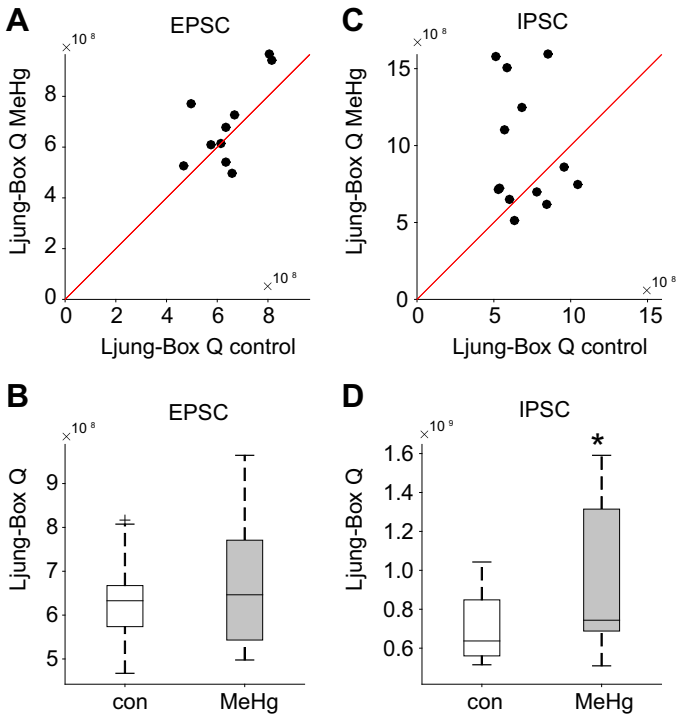

Figure 10. Statistical analysis revealed significant differences in the degree of synchrony in IPSC, but not EPSC recordings. The Ljung-Box, Q factor was used to quantify the degree of cumulative synchrony within the autocovariance functions for IPSC and EPSC recordings, before and after MeHg treatment. *A* and *B*: across the population of sampled neurons ($n = 10$), the Ljung-Box Q factor for EPSCs was not significantly different between control (6.4e8 ± 3.6e7) and MeHg treated conditions (6.8e8 ± 5.2e7). *C* and *D*: however, IPSCs for the sampled neurons ($n = 13$), showed that the degree of synchrony, as measured by the Ljung-Box Q factor, was significantly greater ($P = 0.037$, ANOVA, indicated by *) in the MeHg conditions (9.6e8 ± 1.1e8) compared with control (7.0e8 ± 4.8e7). EPSC, excitatory postsynaptic current; IPSC, inhibitory postsynaptic current; MeHg, methylmercury.

and *C*) with no sign of low-frequency synchrony, as observed in the IPSC traces.

In order to quantify the degree of temporal synchrony within the synaptic current traces, the Ljung-Box Q-factor metric (57) was calculated for EPSC and IPSC traces (Fig. 10).

$$Q = n(n + 2)\sum_{j=1}^{h}\frac{R_j^2}{n-j},$$

where n is the sample size, R is the sample autocorrelation at lag j, h is the number of lags being tested. When control (6.4e8 ± 3.6e7) and MeHg exposed (6.8e8 ± 5.2e7) EPSC recordings were compared ($n = 10$ neurons), there is no significant difference in the cumulative synchrony, as estimated by the Ljung-Box Q-factor (Fig. 10, *A* and *B*). However, IPSCs (Fig. 10, *C* and *D*) showed a significantly greater ($P = 0.037$, ANOVA, $n = 13$ neurons) degree of synchrony as measured by the Ljung-Box Q factor for MeHg conditions (9.6e8 ± 1.1e8) compared with control (7.0e8 ± 4.8e7).

Mercury Exposure Increases Excitability of mPFC Pyramidal Neurons

In addition to synaptic mechanisms that lead to hyperexcitation, changes in the ability of a neuron to generate action potentials in response to inputs can alter excitability. Previous work showed that intrinsic excitability was increased in spinal motor neurons exposed to acute MeHg (41). Therefore, intrinsic action potential firing was also determined in the presence of MeHg, using whole cell current-clamp recording of mPFC excitatory pyramidal neurons. Responses from representative neurons are shown in Fig. 11. Firing rate versus current responses (f-I) were collected across a range of amplitudes of injected current steps (Fig. 11, *A* and *B*). MeHg significantly

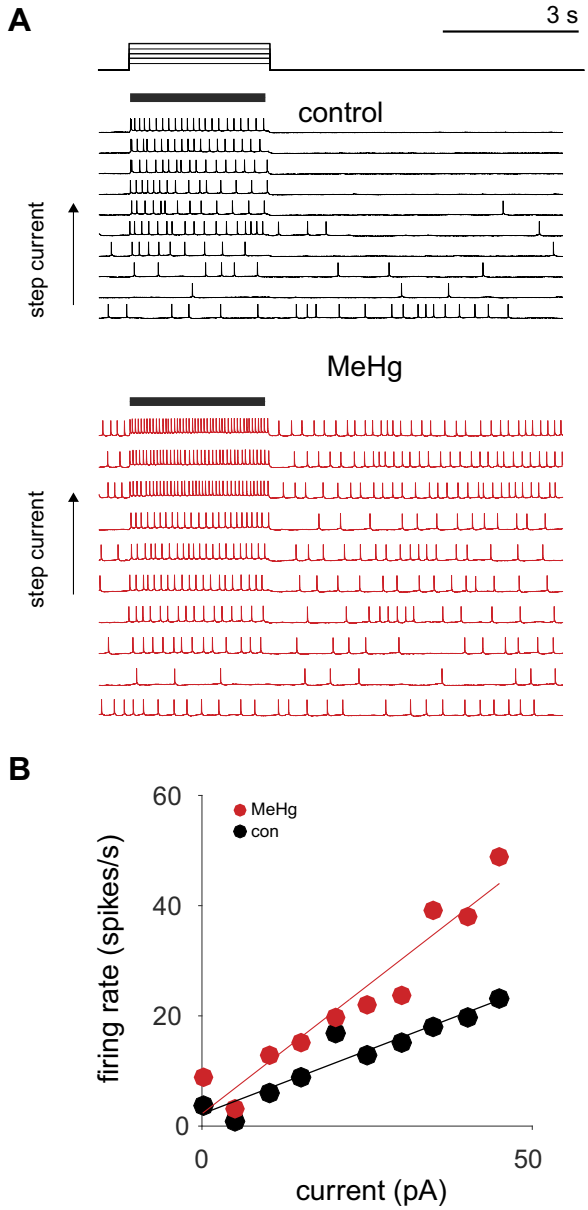

Figure 11. Acute MeHg exposure alters both spontaneous and evoked spiking in excitatory pyramidal mPFC neurons. *A*: whole cell current clamp recording of a representative neuron before (black) and after 15 min MeHg exposure (red). Voltage traces illustrate action potential discharge before and after current pulses of increasing amplitude. *B*: the f-I response curves are shown for estimates of firing rate during the current step periods for a representative neuron. Action potential firing rate as a function of current injection (f-I response gain; slope), was increased as a result of MeHg exposure (black is control, red is MeHg treated). MeHg, methylmercury; mPFC, medial prefrontal cortex.

enhanced the intrinsic excitability of layer 5 excitatory pyramidal neurons of the prelimbic mPFC (Figs. 11 and 12), as revealed through analysis of action potential firing. Voltage traces were compared before and after MeHg to determine the effects on both spontaneous spiking and evoked spiking in response to current pulse injections delivered via the recording electrode (Figs. 11 and 12). Spontaneous spiking significantly increased after MeHg exposure (Fig. 12, *D* and *E*; 0.14 ± 0.08 Hz and 0.6 ± 0.3 Hz, control vs. MeHg; $P = 0.002$, Wilcoxon ranksum).

To analyze neuronal spiking in response to current pulses, the current-to-firing rate transfer function (f-I) was estimated by delivering a range of current amplitudes via the recording electrode. The slope of the f-I curve increased in response to MeHg exposure (Figs. 11*B* and 12, *B* and *C*; 0.35 ± 0.03 Hz/pA and 0.50 ± 0.07 Hz/pA for control and MeHg, respectively; $P = 6.3864e\text{-}05$, Wilcoxon ranksum; $n = 10$ neurons), in addition to an increase in variability. These data indicate that the intrinsic excitability of mPFC pyramidal neurons is increased upon MeHg exposure.

Increased intrinsic excitability could stem from changes in the action potential itself. Therefore, we quantified population averages of action potential metrics for amplitude, duration, and resting potential (Fig. 13). Individual action potential properties were unaltered by MeHg exposure (Fig. 13). The mean resting membrane potential for control (−67 ± 1.8 mV) was not significantly depolarized after MeHg treatment (−65 ± 1.4 mV). In addition, neither action potential amplitude (79.2 ± 5.9 mV and 77.1 ± 5.6 mV for control and MeHg, respectively) nor duration (3.5 ± 0.3 ms and 3.7 ± 0.3 ms for control and MeHg, respectively) were significantly different as a result of MeHg exposure. Therefore, the increased excitability observed above is not a result of direct changes in action potential properties.

DISCUSSION

Disorders affecting the PFC exhibit a range of symptoms, including deficits in cognitive performance, attention, motivation, and emotional impulse control. Although some conditions such as bipolar disorder have been linked to particular genes, other forms of frontotemporal disorder do not correlate with known genetic mutations. Sporadic cases of FTD are 50–70% of those reported (31–35, 58). Environmental toxicant exposure is a known risk factor for symptoms overlapping FTD (59, 60). Mercury exposure has been linked to symptoms expressed in FTD and could either trigger or accelerate FTD symptoms (15, 23–25, 61). Here, we report specific actions of MeHg on mPFC excitatory neurons that indicate a significant shift toward hyperexcitability and synaptic E-I balance disruption.

Intrinsic excitability of prelimbic mPFC layer 5 excitatory neurons was significantly increased in the presence of MeHg. Both spontaneous and electrically evoked action potentials were upregulated after MeHg treatment. Intracellular current injection-evoked action potentials revealed an increase in f-I slope after MeHg exposure, reflecting an increase in action potential discharge in response to the same level of input current. This increase in f-I response gain would result in a greater spiking rate for the same input, producing an overall

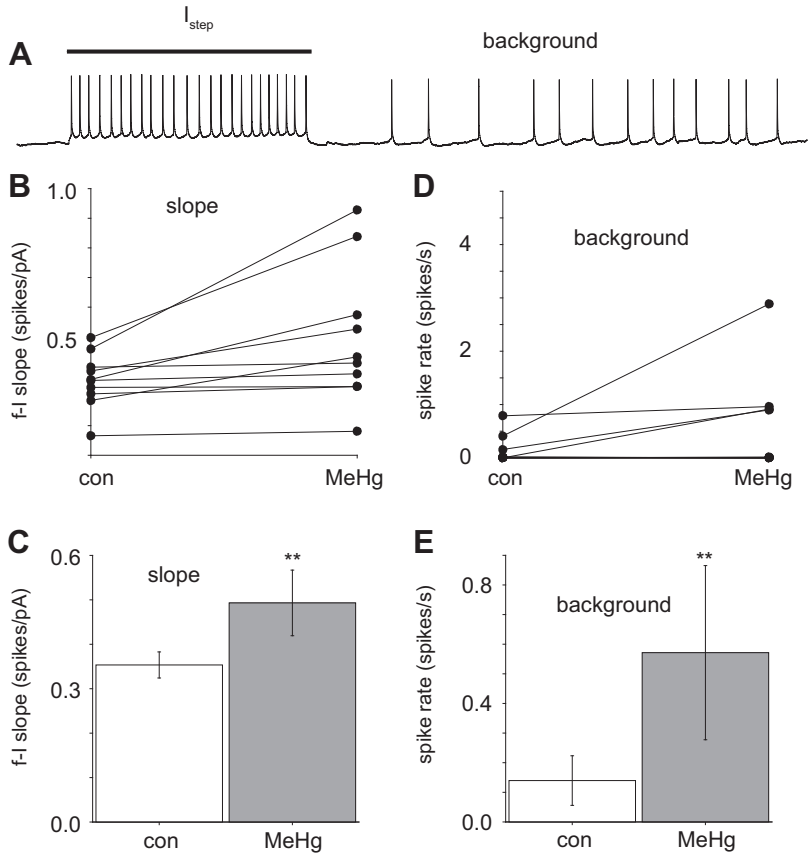

Figure 12. MeHg increased evoked firing rate response gain (f-I slope) and spontaneous background spiking. *A*: representative voltage trace showing action potential discharge in response to a whole cell current clamp recording current step and spontaneous background firing after evoked stimulation. *B* and *C*: across the population of sampled neurons ($n = 10$), there was a significant increase in the response gain or f-I slope after MeHg exposure in a within-same-cell comparison. The f-I response gain increased from 0.35 ± 0.03 Hz/pA to 0.5 ± 0.07 Hz/pA ($P = 6.38e\text{-}05$, Wilcoxon ranksum test) after MeHg exposure. *D* and *E*: MeHg exposure also produced a significant increase in spontaneous background firing ($P = 0.002$, Wilcoxon ranksum test) from 0.14 ± 0.1 Hz to 0.6 ± 0.3 Hz after MeHg treatment. Significant dfferences indicated by **. MeHg, methylmercury.

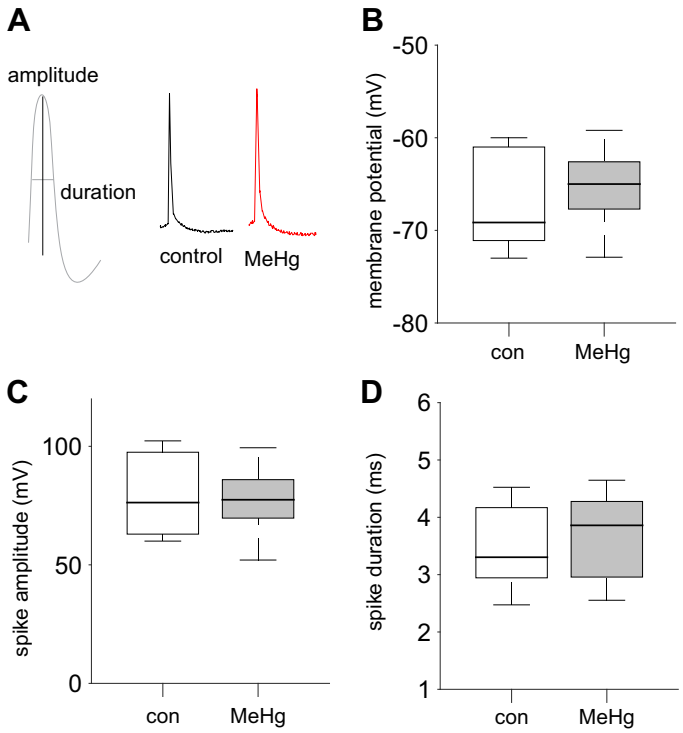

Figure 13. Action potential properties were not significantly altered by MeHg exposure. *A*: representative action potentials for a sample neuron in mPFC before (black) and after MeHg treatment (red). Across all sampled neurons ($n = 10$), action potential duration, amplitude, and resting membrane potential were estimated. *B*: the mean resting membrane potential for control (−67 ± 1.8 mV) was not significantly depolarized after MeHg treatment (−65 ± 1.4 mV). *C*: action potential amplitude was not significantly different after MeHg exposure (79.2 ± 5.9 mV and 77.1 ± 5.6 mV, respectively). *D*: the duration, or full-width at half-height, of the action potentials were also not significantly different in control (3.5 ± 0.3 ms) and MeHg (3.7 ± 0.3 ms) conditions. MeHg, methylmercury; mPFC, medial prefrontal cortex.

increase the excitability across the mPFC. This shift toward hyperexcitability is independent of changes in synaptic inputs, because depolarization was achieved through current-clamp rather than extracellular stimulation. Individual action potentials were unaffected by the presence of MeHg with no apparent change in action potential properties. Inspection of phase portraits (not shown) also support the idea that action potential dynamics were unchanged. One interesting possibility is that increased spike frequency could stem from a MeHg-induced reduction in a hyperpolarizing or shunting current. We did not observe a depolarization of the resting potential, arguing against a reduction in tonic hyperpolarizing conductances, but it will be interesting in the future to determine whether MeHg regulates an activity-dependent hyperpolarizing or shunting conductance as a mechanism for the increased spike rates observed here.

Acute MeHg exposure also shifted E-I balance in prelimbic mPFC layer 5 excitatory pyramidal neurons. E-I balance—the ratio of excitatory to inhibitory synaptic drive—helps establish the intrinsic excitability of the cortex (62–65). After 15 min of MeHg treatment, synaptic E-I balance was shifted toward increased excitation, since EPSC frequency was increased without a concomitant change in IPSC frequency. Neither EPSC nor IPSC amplitudes were changed by mercury exposure. Together, these data are consistent with a presynaptic rather than postsynaptic mechanism, raising the question of whether the increased EPSC frequency is a consequence of increased probability of release. Arguing against this potential mechanism, changes in release probability are unlikely to account for the observed increase in spontaneous EPSC frequency since PPR was increased after acute exposure to MeHg, suggesting a decrease in release probability. Given that increased EPSC frequency appeared after only 15 min of exposure to MeHg, it is also unlikely that these effects were a result of formation of new synapses.

The observed increase in EPSC event frequency in the absence of elevated probability of release could be a result of MeHg-induced effects on spontaneous but not evoked glutamate release. Evoked release is tightly coupled to presynaptic action potentials, while spontaneous release occurs in the absence of presynaptic action potentials. Spontaneous and evoked synaptic transmission are mechanistically separable and can be modulated independently (66). Both forms of transmitter release depend on presynaptic calcium; however, spontaneous and evoked events differ in the timing of release in response to calcium, levels of presynaptic calcium required, and mechanisms of presynaptic calcium increase. Interestingly, spontaneous release at excitatory and inhibitory synapses appears to be sensitive to different sources of intracellular calcium (66). Spontaneous and evoked glutamate release also activate distinct populations of postsynaptic glutamate receptors in the postsynaptic density (67, 68). The data presented here show that EPSC amplitude was unchanged by MeHg for both spontaneous and evoked release, arguing against a postsynaptic effect for either type of synaptic transmission. The relationship between spontaneous and evoked release appears to vary across different types of synapses (66), which could contribute to differences observed between the effects of MeHg on different types of neurons.

Overall synaptic activity in mPFC was increased in the presence of MeHg since both EPSC and IPSC charge were significantly increased. However, there was no observable effect on spontaneous or evoked EPSC or IPSC amplitude, suggesting that individual synaptic responses were unchanged. Analysis of synaptic current charge does not rely on measuring individual, isolated current deflections. Therefore, higher synaptic charge could result from increased overlap of synaptic events, without an apparent change in amplitudes of single events. For excitatory synapses, increased EPSC frequency contributes to increased excitatory charge. Since inhibitory currents did not display increased frequency, inhibitory charge must be produced through an alternative mechanism. Interestingly, inhibitory currents displayed significant increases in synchrony after MeHg exposure: this represents a plausible mechanism for increased inhibitory charge. Together, these observations demonstrate that MeHg exposure alters the temporal organization of synaptic activation in mPFC.

We do not yet know the underlying mechanisms of the observed MeHg-induced increase in IPSC synchrony. One interesting possibility is that MeHg could regulate gap junctions to increase efficiency of electrical coupling between inhibitory neurons. Inhibitory interneurons in the cerebral cortex are coupled to other inhibitory neurons of the same subtype through both chemical and electrical synapses (69–71). It is well-established that gap junctions contribute to

synchronization of electrically coupled interneurons (69). In addition, gap junction-mediated electrical coupling is plastic and can be regulated by a variety of mechanisms, including calcium signaling, neuronal activity, and some psychostimulants (71). It would be interesting in the future to determine whether acute MeHg exposure increases IPSC frequency through modulation of electrical coupling between specific types of inhibitory neurons.

Overall, the data presented here are consistent with the idea that acute MeHg exposure interferes with prelimbic mPFC network function through disruption of normal patterns of synaptic activity, E-I balance and input-output relationships within layer 5 excitatory neurons. This represents a significant impairment to mPFC circuits that underlie emotion and cognition and are likely to contribute to the development of symptoms of erethism and similar MeHg-induced neuropsychological pathologies. These disruptions in mPFC networks may also contribute to cognitive dysfunction in other disorders, such as frontotemporal disorders and dementia, with cognitive impairment linked to mPFC dysfunction.

DATA AVAILABILITY

Data will be made available upon reasonable request.

DISCLOSURES

No conflicts of interest, financial or otherwise, are declared by the authors.

AUTHOR CONTRIBUTIONS

M.P.S. conceived and designed research; M.P.S. performed experiments; M.P.S. analyzed data; M.P.S. and S.L.S. interpreted results of experiments; M.P.S. prepared figures; M.P.S. and S.L.S. drafted manuscript; M.P.S. and S.L.S. edited and revised manuscript; M.P.S. and S.L.S. approved final version of manuscript.

REFERENCES

1. **Colon-Rodriguez A**, **Hannon HE**, **Atchison WD.** Effects of methylmercury on spinal cord afferents and efferents-a review. *Neurotoxicology* 60: 308–320, 2017. doi:10.1016/j.neuro.2016.12.007.
2. **Clarkson TW.** Environmental contaminants in the food chain. *Am J Clin Nutr* 61, *Suppl* 3: 682S–686S, 1995. doi:10.1093/ajcn/61.3.682S.
3. **Clarkson TW**, **Magos L.** The toxicology of mercury and its chemical compounds. *Crit Rev Toxicol* 36: 609–662, 2006. doi:10.1080/10408440600845619.
4. **Clarkson TW.** The three modern faces of mercury. *Environ Health Perspect* 110, *Suppl* 1: 11–23, 2002. doi:10.1289/ehp.02110s111.
5. **Bakir F**, **Damluji SF**, **Amin-Zaki L**, **Murtadha M**, **Khalidi A**, **Al-Rawi NY**, **Tikriti S**, **Dahahir HI**, **Clarkson TW**, **Smith JC**, **Doherty RA.** Methylmercury poisoning in Iraq. *Science* 181: 230–241, 1973. doi:10.1126/science.181.4096.230.
6. **Eto K.** Pathology of Minamata disease. *Toxicol Pathol* 25: 614–623, 1997 [Erratum in *Toxicol Pathol* 26: 741, 1998]. doi:10.1177/019262339702500612.
7. **de Paula Arrifano G**, **Crespo-Lopez ME**, **Lopes-Araújo A**, **Santos-Sacramento L**, **Barthelemy JL**, **de Nazaré CGL**, **Freitas LGR**, **Augusto-Oliveira M.** Neurotoxicity and the global worst pollutants: astroglial involvement in arsenic, lead, and mercury intoxication. *Neurochem Res* 48: 1047–1065, 2023. doi:10.1007/s11064-022-03725-7.
8. **Takahashi T**, **Shimohata T.** Vascular dysfunction induced by mercury exposure. *Int J Mol Sci* 20: 2435, 2019. doi:10.3390/ijms20102435.
9. **Aschner M**, **Aschner JL.** Mercury neurotoxicity: mechanisms of blood-brain barrier transport. *Neurosci Biobehav Rev* 14: 169–176, 1990. doi:10.1016/s0149-7634(05)80217-9.
10. **Gochfeld M.** Cases of mercury exposure, bioavailability, and absorption. *Ecotoxicol Environ Saf* 56: 174–179, 2003. doi:10.1016/s0147-6513(03)00060-5.
11. **Clarkson TW.** The toxicology of mercury. *Crit Rev Clin Lab Sci* 34: 369–403, 1997. doi:10.3109/10408369708998098.
12. **Miura K**, **Imura N.** Mechanism of methylmercury cytotoxicity. *Crit Rev Toxicol* 18: 161–188, 1987. doi:10.3109/10408448709089860.
13. **Kajiwara Y**, **Yasutake A**, **Adachi T**, **Hirayama K.** Methylmercury transport across the placenta via neutral amino acid carrier. *Arch Toxicol* 70: 310–314, 1996. doi:10.1007/s002040050279.
14. **Simmons-Willis TA**, **Koh AS**, **Clarkson TW**, **Ballatori N.** Transport of a neurotoxicant by molecular mimicry: the methylmercury-L-cysteine complex is a substrate for human L-type large neutral amino acid transporter (LAT) 1 and LAT2. *Biochem J* 367: 239–246, 2002. doi:10.1042/BJ20020841.
15. **Jackson AC.** Chronic neurological disease due to methylmercury poisoning. *Can J Neurol Sci* 45: 620–623, 2018. doi:10.1017/cjn.2018.323.
16. **Santos-Sacramento L**, **Arrifano GP**, **Lopes-Araújo A**, **Augusto-Oliveira M**, **Albuquerque-Santos R**, **Takeda PY**, **Souza-Monteiro JR**, **Macchi BM**, **do Nascimento JLM**, **Lima RR**, **Crespo-Lopez ME.** Human neurotoxicity of mercury in the Amazon: A scoping review with insights and critical considerations. *Ecotoxicol Environ Saf* 208: 111686, 2021. doi:10.1016/j.ecoenv.2020.111686.
17. **Cercy SP**, **Wankmuller MM.** Cognitive dysfunction associated with elemental mercury ingestion and inhalation: a case study. *Appl Neuropsychol* 15: 79–91, 2008. doi:10.1080/09084280801917889.
18. **Adams CR**, **Ziegler DK**, **Lin JT.** Mercury intoxication simulating amyotrophic lateral sclerosis. *JAMA* 250: 642–643, 1983.
19. **Callaghan B**, **Feldman D**, **Gruis K**, **Feldman E.** The association of exposure to lead, mercury, and selenium and the development of amyotrophic lateral sclerosis and the epigenetic implications. *Neurodegener Dis* 8: 1–8, 2011. doi:10.1159/000315405.
20. **Hansen JC**, **Reske-Nielsen E**, **Thorlacius-Ussing O**, **Rungby J**, **Danscher G.** Distribution of dietary mercury in a dog. Quantitation and localization of total mercury in organs and central nervous system. *Sci Total Environ* 78: 23–43, 1989. doi:10.1016/0048-9697(89)90020-x.
21. **Johnson FO**, **Atchison WD.** The role of environmental mercury, lead and pesticide exposure in development of amyotrophic lateral sclerosis. *Neurotoxicology* 30: 761–765, 2009. doi:10.1016/j.neuro.2009.07.010.
22. **Praline J**, **Guennoc A-M**, **Limousin N**, **Hallak H**, **de Toffol B**, **Corcia P.** ALS and mercury intoxication: a relationship? *Clin Neurol Neurosurg* 109: 880–883, 2007. doi:10.1016/j.clineuro.2007.07.008.
23. **Maghazaji HI.** Psychiatric aspects of methylmercury poisoning. *J Neurol Neurosurg Psychiatry* 37: 954–958, 1974. doi:10.1136/jnnp.37.8.954.
24. **Myers GJ**, **Davidson PW**, **Cox C**, **Shamlaye C**, **Cernichiari E**, **Clarkson TW.** Twenty-seven years studying the human neurotoxicity of methylmercury exposure. *Environ Res* 83: 275–285, 2000. doi:10.1006/enrs.2000.4065.
25. **Yokoo EM**, **Valente JG**, **Grattan L**, **Schmidt SL**, **Platt I**, **Silbergeld EK.** Low level methylmercury exposure affects neuropsychological function in adults. *Environ Health* 2: 8, 2003. doi:10.1186/1476-069X-2-8.
26. **Rustam H**, **Hamdi T.** Methyl mercury poisoning in Iraq. A neurological study. *Brain* 97: 500–510, 1974.
27. **Møller-Madsen B**, **Danscher G.** Localization of mercury in CNS of the rat. IV. The effect of selenium on orally administered organic and inorganic mercury. *Toxicol Appl Pharmacol* 108: 457–473, 1991. doi:10.1016/0041-008x(91)90092-s.
28. **Møller-Madsen B.** Localization of mercury in CNS of the rat. II. Intraperitoneal injection of methylmercuric chloride (CH3HgCl) and mercuric chloride (HgCl2). *Toxicol Appl Pharmacol* 103: 303–323, 1990. doi:10.1016/0041-008x(90)90232-j.
29. **Warfvinge K.** Mercury distribution in the mouse brain after mercury vapour exposure. *Int J Exp Pathol* 76: 29–35, 1995.
30. **Eyl TB.** Methyl mercury poisoning in fish and human beings. *Clin Toxicol* 4: 291–296, 1971. doi:10.3109/15563657108990969.
31. **Sjögren M**, **Andersen C.** Frontotemporal dementia–a brief review. *Mech Ageing Dev* 127: 180–187, 2006. doi:10.1016/j.mad.2005.09.015.
32. **Grossman M**, **Seeley WW**, **Boxer AL**, **Hillis AE**, **Knopman DS**, **Ljubenov PA**, **Miller B**, **Piguet O**, **Rademakers R**, **Whitwell JL**, **Zetterberg H**, **van Swieten JC.** Frontotemporal lobar degeneration. *Nat Rev Dis Primers* 9: 40, 2023. doi:10.1038/s41572-023-00447-0.

33. **Waldö ML.** The frontotemporal dementias. *Psychiatr Clin North Am* 38: 193–209, 2015. doi:10.1016/j.psc.2015.02.001.
34. **Mori K**, **Ikeda M.** Biological basis and psychiatric symptoms in frontotemporal dementia. *Psychiatry Clin Neurosci* 76: 351–360, 2022. doi:10.1111/pcn.13375.
35. **Golimstok A**, **Cámpora N**, **Rojas JI**, **Fernandez MC**, **Elizondo C**, **Soriano E**, **Cristiano E.** Cardiovascular risk factors and frontotemporal dementia: a case-control study. *Transl Neurodegener* 3: 13, 2014. doi:10.1186/2047-9158-3-13.
36. **Landrigan PJ**, **Sonawane B**, **Butler RN**, **Trasande L**, **Callan R**, **Droller D.** Early environmental origins of neurodegenerative disease in later life. *Environ Health Perspect* 113: 1230–1233, 2005. doi:10.1289/ehp.7571.
37. **Elbaz A**, **Dufouil C**, **Alpérovitch A.** Interaction between genes and environment in neurodegenerative diseases. *C R Biol* 330: 318–328, 2007. doi:10.1016/j.crvi.2007.02.018.
38. **Migliore L**, **Coppedè F.** Genetics, environmental factors and the emerging role of epigenetics in neurodegenerative diseases. *Mutat Res* 667: 82–97, 2009. doi:10.1016/j.mrfmmm.2008.10.011.
39. **Teixeira FB**, **de Oliveira ACA**, **Leão LKR**, **Fagundes NCF**, **Fernandes RM**, **Fernandes LMP**, **da Silva MCF**, **Amado LL**, **Sagica FES**, **de Oliveira EHC**, **Crespo-Lopez ME**, **Maia CSF**, **Lima RR.** Exposure to inorganic mercury causes oxidative stress, cell death, and functional deficits in the motor cortex. *Front Mol Neurosci* 11: 125, 2018. doi:10.3389/fnmol.2018.00125.
40. **Cariccio VL**, **Samà A**, **Bramanti P**, **Mazzon E.** Mercury involvement in neuronal damage and in neurodegenerative diseases. *Biol Trace Elem Res* 187: 341–356, 2019. doi:10.1007/s12011-018-1380-4.
41. **Sceniak MP**, **Spitsbergen JB**, **Sabo SL**, **Yuan Y**, **Atchison WD.** Acute neurotoxicant exposure induces hyperexcitability in mouse lumbar spinal motor neurons. *J Neurophysiol* 123: 1448–1459, 2020. doi:10.1152/jn.00775.2019.
42. **Yuan Y**, **Atchison WD.** Electrophysiological studies of neurotoxicants on central synaptic transmission in acutely isolated brain slices. *Curr Protoc Toxicol* Chapter 11: Unit11.11, 2003. doi:10.1002/0471140856.tx1111s17.
43. **Ting JT**, **Lee BR**, **Chong P**, **Soler-Llavina G**, **Cobbs C**, **Koch C**, **Zeng H**, **Lein E.** Preparation of acute brain slices using an optimized *N*-methyl-D-glucamine protective recovery method. *J Vis Exp* 132: 53825, 2018. doi:10.3791/53825.
44. **Sceniak MP**, **Maciver MB.** Cellular actions of urethane on rat visual cortical neurons in vitro. *J Neurophysiol* 95: 3865–3874, 2006. doi:10.1152/jn.01196.2005.
45. **Sceniak MP**, **Sabo SL.** Modulation of firing rate by background synaptic noise statistics in rat visual cortical neurons. *J Neurophysiol* 104: 2792–2805, 2010. doi:10.1152/jn.00023.2010.
46. **Sceniak MP**, **Lang M**, **Enomoto AC**, **James Howell C**, **Hermes DJ**, **Katz DM.** Mechanisms of functional hypoconnectivity in the medial prefrontal cortex of Mecp2 null mice. *Cereb Cortex* 26: 1938–1956, 2016. doi:10.1093/cercor/bhv002.
47. **Yuan Y**, **Atchison WD.** Methylmercury acts at multiple sites to block hippocampal synaptic transmission. *J Pharmacol Exp Ther* 275: 1308–1316, 1995.
48. **Yuan Y**, **Atchison WD.** Disruption by methylmercury of membrane excitability and synaptic transmission of CA1 neurons in hippocampal slices of the rat. *Toxicol Appl Pharmacol* 120: 203–215, 1993. doi:10.1006/taap.1993.1104.
49. **Atchison WD**, **Hare MF.** Mechanisms of methylmercury-induced neurotoxicity. *FASEB J* 8: 622–629, 1994. doi:10.1096/fasebj.8.9.7516300.
50. **Yuan Y**, **Atchison WD.** Action of methylmercury on GABA(A) receptor-mediated inhibitory synaptic transmission is primarily responsible for its early stimulatory effects on hippocampal CA1 excitatory synaptic transmission. *J Pharmacol Exp Ther* 282: 64–73, 1997.
51. **Yuan Y**, **Atchison WD.** Methylmercury differentially affects GABA(A) receptor-mediated spontaneous IPSCs in Purkinje and granule cells of rat cerebellar slices. *J Physiol* 550: 191–204, 2003. doi:10.1113/jphysiol.2003.040543.
52. **Kruse AO**, **Bustillo JR.** Glutamatergic dysfunction in schizophrenia. *Transl Psychiatry* 12: 500, 2022. doi:10.1038/s41398-022-02253-w.
53. **Benussi A**, **Alberici A**, **Buratti E**, **Ghidoni R**, **Gardoni F**, **Di Luca M**, **Padovani A**, **Borroni B.** Toward a glutamate hypothesis of frontotemporal dementia. *Front Neurosci* 13: 304, 2019. doi:10.3389/fnins.2019.00304.
54. **Butler PM**, **Chiong W.** Neurodegenerative disorders of the human frontal lobes. *Handb Clin Neurol* 163: 391–410, 2019. doi:10.1016/B978-0-12-804281-6.00021-5.
55. **Jobson DD**, **Hase Y**, **Clarkson AN**, **Kalaria RN.** The role of the medial prefrontal cortex in cognition, ageing and dementia. *Brain Commun* 3: fcab125, 2021. doi:10.1093/braincomms/fcab125.
56. **Duman RS.** Neurobiology of stress, depression, and rapid acting antidepressants: remodeling synaptic connections. *Depress Anxiety* 31: 291–296, 2014. doi:10.1002/da.22227.
57. **Ljung GM**, **Box GEP.** On a measure of lack of fit in time series models. *Biometrika* 65: 297–303, 1978. doi:10.1093/biomet/65.2.297.
58. **Rasmussen H**, **Stordal E**, **Rosness TA.** Risk factors for frontotemporal dementia. *Tidsskr Nor Legeforen* 138: 14, 2018. doi:10.4045/tidsskr.17.0763.
59. **Adani G**, **Filippini T**, **Garuti C**, **Malavolti M**, **Vinceti G**, **Zamboni G**, **Tondelli M**, **Galli C**, **Costa M**, **Vinceti M**, **Chiari A.** Environmental risk factors for early-onset Alzheimer's dementia and frontotemporal dementia: a case-control study in Northern Italy. *Int J Environ Res Public Health* 17: 7941, 2020. doi:10.3390/ijerph17217941.
60. **Silman AK**, **Chhabria R**, **Hafzalla GW**, **Giffin L**, **Kucharski K**, **Myers K**, **Culquichicón C**, **Montero S**, **Lescano AG**, **Vega CM**, **Fernandez LE**, **Silman MR**, **Kane MJ**, **Sanders JW.** Impairment in working memory and executive function associated with mercury exposure in indigenous populations in Upper Amazonian Peru. *Int J Environ Res Public Health* 19: 10989, 2022. doi:10.3390/ijerph191710989.
61. **Myers GJ**, **Thurston SW**, **Pearson AT**, **Davidson PW**, **Cox C**, **Shamlaye CF**, **Cernichiari E**, **Clarkson TW.** Postnatal exposure to methyl mercury from fish consumption: a review and new data from the Seychelles Child Development Study. *Neurotoxicology* 30: 338–349, 2009. doi:10.1016/j.neuro.2009.01.005.
62. **Léger J-F**, **Stern EA**, **Aertsen A**, **Heck D.** Synaptic integration in rat frontal cortex shaped by network activity. *J Neurophysiol* 93: 281–293, 2005. doi:10.1152/jn.00067.2003.
63. **Maffei A**, **Nelson SB**, **Turrigiano GG.** Selective reconfiguration of layer 4 visual cortical circuitry by visual deprivation. *Nat Neurosci* 7: 1353–1359, 2004. doi:10.1038/nn1351.
64. **Trevelyan AJ**, **Watkinson O.** Does inhibition balance excitation in neocortex? *Prog Biophys Mol Biol* 87: 109–143, 2005. doi:10.1016/j.pbiomolbio.2004.06.008.
65. **Xing J**, **Gerstein GL.** Networks with lateral connectivity. I. dynamic properties mediated by the balance of intrinsic excitation and inhibition. *J Neurophysiol* 75: 184–199, 1996. doi:10.1152/jn.1996.75.1.184.
66. **Kavalali ET.** The mechanisms and functions of spontaneous neurotransmitter release. *Nat Rev Neurosci* 16: 5–16, 2015. doi:10.1038/nrn3875.
67. **Atasoy D**, **Ertunc M**, **Moulder KL**, **Blackwell J**, **Chung C**, **Su J**, **Kavalali ET.** Spontaneous and evoked glutamate release activates two populations of NMDA receptors with limited overlap. *J Neurosci* 28: 10151–10166, 2008. doi:10.1523/JNEUROSCI.2432-08.2008.
68. **Sara Y**, **Bal M**, **Adachi M**, **Monteggia LM**, **Kavalali ET.** Use-dependent AMPA receptor block reveals segregation of spontaneous and evoked glutamatergic neurotransmission. *J Neurosci* 31: 5378–5382, 2011. doi:10.1523/JNEUROSCI.5234-10.2011.
69. **Bennett MVL**, **Zukin RS.** Electrical coupling and neuronal synchronization in the mammalian brain. *Neuron* 41: 495–511, 2004. doi:10.1016/s0896-6273(04)00043-1.
70. **Hestrin S**, **Galarreta M.** Electrical synapses define networks of neocortical GABAergic neurons. *Trends Neurosci* 28: 304–309, 2005. doi:10.1016/j.tins.2005.04.001.
71. **Coulon P**, **Landisman CE.** The potential role of gap junctional plasticity in the regulation of state. *Neuron* 93: 1275–1295, 2017. doi:10.1016/j.neuron.2017.02.041.